Received: 17 June 2016 | Revised: 18 July 2017 | Accepted: 18 September 2017

DOI: 10.1002/ppp.1968

WILEY

RESEARCH ARTICLE

Kinematic investigations on the Furggwanghorn Rock Glacier, Switzerland

Thomas Buchli[1] | Andrew Kos[1,2] | Philippe Limpach[3] | Kaspar Merz[4] | Xiaohai Zhou[5]* | Sarah M. Springman[1]

[1] Institute for Geotechnical Engineering, Zürich, Switzerland

[2] Terrasense Switzerland Ltd, Buchs, SG, Switzerland

[3] Institute of Geodesy and Photogrammetry, Zürich, Switzerland

[4] Institute of Geophysics, Zurich, Switzerland

[5] Laboratory for Multiscale Studies in Building Physics, Dübendorf, Switzerland

Correspondence
Thomas Buchli, Institute for Geotechnical Engineering, ETH Zürich, Switzerland.
Email: thomas.buchli@igt.baug.ethz.ch

Funding information
ETH Research Commission, Grant/Award Number: CHI-01 09-03

Abstract

Many thermo-hydro-mechanical parameters and their interactions influence the creep behaviour of rock glaciers, with the result that the kinematics of rock glaciers are complex and not fully understood. An interdisciplinary project began in 2010 to investigate the physical ground conditions and any climatic dependence of a fast-moving rock glacier below the Furggwanghorn peak, in the Turtmann Valley of the Swiss Alps. Remote sensing and subsurface instrumentation (in-place inclinometers and temperature sensors), together with ground and airborne geophysical methods, reveal the creep rate and the hydrological and thermal conditions of the rock glacier. The Furggwanghorn rock glacier exhibits displacements in the order of metres per year and showed substantial surface changes at a minimal ground temperature slightly below 0°C. A detailed three-dimensional kinematic ground model shows the internal structure and shear surfaces, indicating past creep behaviour and failure mechanisms. The results suggest that observed seasonal changes in the creep rate of the rock glacier did not depend directly on the temperature at depth, but were very likely controlled by hydrological processes.

KEYWORDS

3-D kinematic ground model, failure mechanism, inclinometer, rock glaciers, terrestrial laser scanning, terrestrial radar interferometric measurements

1 | INTRODUCTION

Understanding the thermal state and the kinematic behaviour of rock glaciers is essential for assessing hazards and limiting risks to infrastructure and human activities. Several past mass-movement events have occurred in warm rock glaciers (eg, Val Pola in Italy in 1997, and the Bérard rock glacier in France; [1–4]), where heavy rainfall can trigger downslope transport of large volumes of soil.[5]

Several studies connect rising mean annual air temperature and accelerating creep velocity of alpine rock glaciers (eg, [6,7]). The increase in velocity is often attributed to a change in the thermal regime of the ground, induced by climate change.[8–11] Loss of ice content and increase in water content reduce the shear strength of the ice-soil mixture (eg, [12,13]). This is due either to lower cohesion between the soil particles,[14] or higher pore pressure through snowmelt or subsurface water flows, which may cause the rock glacier to become locally unstable in extreme cases.[15] The disappearance of ice within various parts of rock glaciers may strongly affect their geomorphology in the long term, due to differential rates of downslope creep and surface settlement features due to ice volume loss, and their stability during degradation. However, few studies have measured internal movements in rock glaciers (eg, [16–18]).

Most studies of rock glacier kinematics concentrate on surface movements, and neglect internal movements and failure mechanisms. Only a few studies have measured internal movements (eg, [16–18]), which are essential for investigating rock glacier instability. As result, an interdisciplinary project was started in 2010 to investigate the behaviour of the Furggwanghorn rock glacier in the Turtmann valley of the Swiss Alps.[19–22] Its goal was to improve knowledge about the internal processes and kinematics, and thermo-hydro-mechanical coupling.

The main aim of this study is to increase understanding of the thermal, hydrological and geotechnical processes in the complex kinematic system of the Furggwanghorn rock glacier. Specifically, it considers four questions: (1) How and where does the rock glacier move? (2) Which areas remain stable in geotechnical terms? (3) How fast and in which direction are the movements? (4) What triggers or

*Formerly at Institute of Environmental Engineering, ETH Zurich, Switzerland.

influences them? These questions are addressed by assembling and integrating different sources of information and comparing the results of the measuring methods applied.

1.1 | Study site

The Furggwanghorn rock glacier in the Turtmann valley (Valais, Switzerland; Figure 1) was selected for this study because of the relatively high creep rates and the visible changes in its surface from year to year. The rock glacier has exhibited significant geomorphological changes over the observation period (1993–2016), including extension and deepening of depression zones at the root, allowing unique insights into its kinematic behaviour and how it is affected by thermal and hydrological coupling. Typically, the surface of the rock glacier slumps as ice melts and the front and side slopes may flatten.

The rock glacier has an east-southeast to west-northwest orientation. Its lithology comprises mainly schist and gneiss.[21,23] Merz et al.[24] identified four active rock glacier lobes overlying older deposits, delineated from ground penetrating radar (GPR) profiles, inferring a bowl-shaped structure in the bedrock that reaches a maximum depth of about 48 m in the central part. The rock glacier volume was estimated to be 910 000 m^3. It can be divided into four different areas (Figure 1a, b). (1) The root zone, where the debris eroded from the Furggwanghorn peak is deposited on a slope of around 35°, supplies rock debris for any future extension of the rock glacier. (2) The depression zone, which lies directly downslope of the root zone, is characterised by high rates of creep deformation and by rapid surface changes. It is predicted that the depression zone will extend in the future, and other depressions will develop. (3) The main flow zone is characterised by translational movement rates of up to several metres per year. The transported rock debris consists of a well-graded mixture of fine-grained soil up to boulders of 2–3 m in size. (4) The front zone is where local downslope movements occur regularly in the frontal zone of the rock glacier.[25] It is hypothesised that the underlying year-round creep

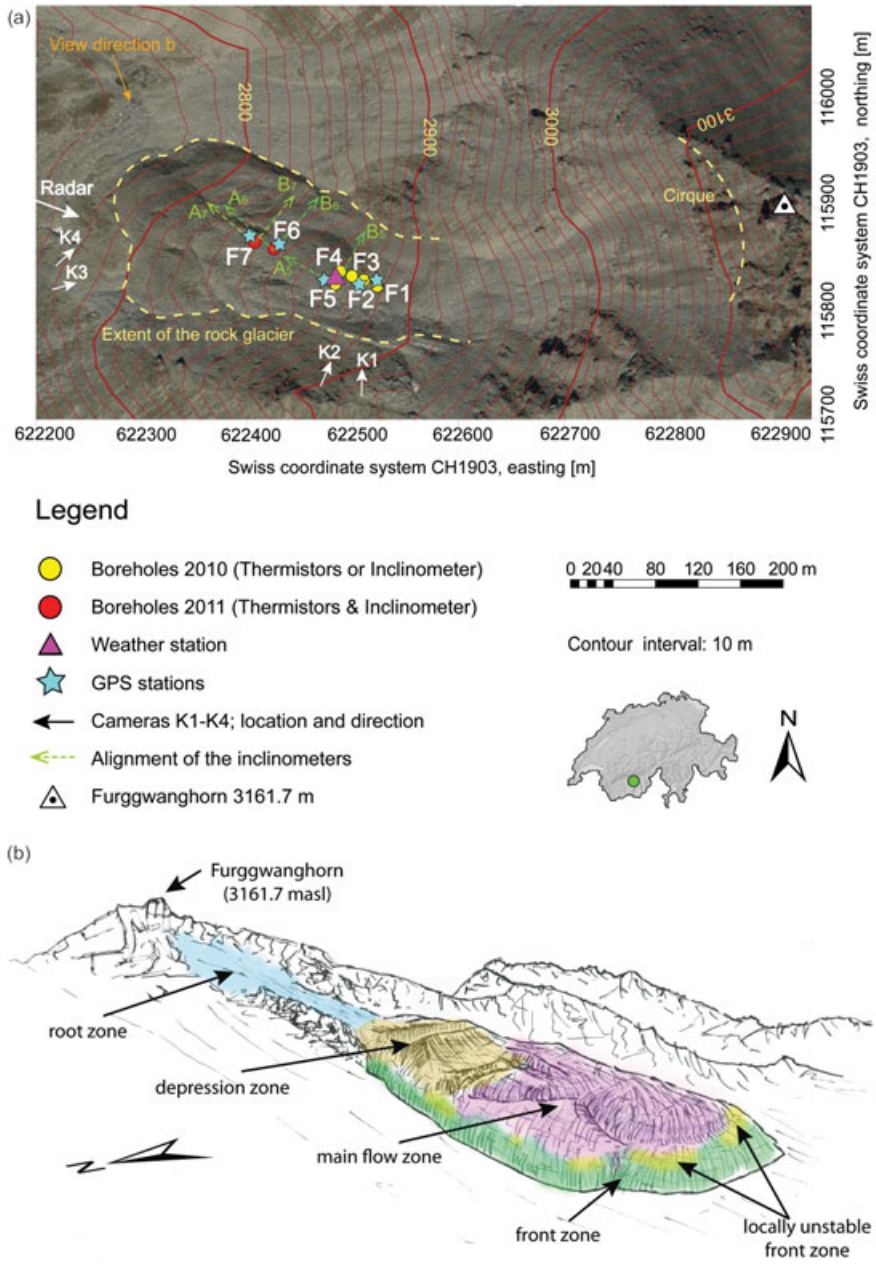

FIGURE 1 Maps of the rock glacier below the Furggwanghorn peak. (a) Orthoimage (adapted after Swisstopo) showing the positions of the boreholes and the monitoring instruments. (b) Oblique schematic sketch of the rock glacier delineating the four main morphological areas (drawn by Th. Buchli). Inset map shows location of study site within Switzerland [Colour figure can be viewed at wileyonlinelibrary.com]

movements in the rock glacier body steepen the front until local failure events occur periodically.[19] It is further postulated, based on field observations, that the front movements are seasonally dependent, with a different failure mechanism operating during thaw periods.

2 | METHODS

The internal structure of the rock glacier, including potential active and former shear zones, was inferred from helicopter ground penetrating radar (H-GPR), and seismic and geoelectric methods.[24,26,27] Periodic and continuous observations were carried out at different surface locations using a combination of terrestrial radar interferometry (TRI), terrestrial laser scanning (TLS, eg, light detection and ranging LiDAR), GPS measurements and digital photography. Automatic inclinometers and thermistors were used to investigate the kinematic and thermal conditions within the rock glacier over 5 years. Instrument locations are shown in Figure 1.

2.1 | Terrestrial laser scanning

2.1.1 | Measurements

High-resolution digital elevation models (DEMs) were constructed from point cloud datasets acquired during measurement campaigns between 2011 and 2015 using an Optech ILRIS-LR terrestrial laser scanner ([28–30]). Laser scans representing the surface of the rock glacier (Supplementary Information, Table S2) were acquired from a number of locations for each year. The commercial software package Polyworks™ (IMAlign and IMsurvey from InnovMetric, http://www.innovmetric.com/) was used to process point clouds, which were translated into the Swiss coordinate system CH1903+,[31] to compare annual surface change of the rock glacier. The point cloud from September 2011 was used as a reference to align the remaining point clouds, together with features such as sharp edges on steep surrounding rock walls (assumed to be stable due to the lack of fresh rockfall debris). Points representing the rock glacier surface were not used in the alignment process. The alignment error is estimated at 23–35 mm and is derived from the sum of the instrumental accuracy (18–30 mm per 600 m range) and the alignment error (average = 5.0 mm).

2.1.2 | Data post-processing

Displacement magnitudes cannot yet be calculated in a plane direction from the point clouds determined and aligned from TLS measurements by using an image correlation method. The point clouds need to be standardised first to define a discrete surface for each measuring campaign. The post-processing is described in Table S1.

2.1.3 | Image correlation analysis of the post-processed TLS data

Points on the three-dimensional (3-D) surface of a rock glacier move simultaneously in vertical and horizontal directions. When the movements are large, correlations between points from different years become inaccurate. Although large boulders can be identified easily between the different measurements, specific points in smooth areas are difficult to correlate without obvious reference points. Displacements were determined in horizontal and vertical directions.

The change in surface height can be calculated by comparing *z*-values for the respective periods (see Supporting Information, TLS data post processing, step e). The shift in plane direction was calculated using a MATLAB®-based optical method called GeoPIV (PIV = particle image velocimetry[32,33]) on the hillshade rasters for the years 2011–15.

The GeoPIV method cannot analyse hillshade images with white areas (no data available, see Table S1, step f). The program interprets these zones as gray scale, and not as areas without data. Therefore, the unadjusted surface (Table S1, step d) was used for image processing. The calculated displacement vectors were then deleted if they were inside the white regions.

2.2 | Radar

The rock glacier front was measured using terrestrial radar interferometry (Table S3) during specific periods in summer and autumn to determine spatial displacement fields at high temporal resolution and rates of movement. Radar images were acquired for each of nine campaigns, with a real aperture, portable radar interferometer, operating with a central frequency of 17.2 GHz,[34] at either 5 or 10 min intervals and lasting approximately 24 hours. A hard disk error resulted in only ~8 hours of measured data being recorded in August 2013.

Consecutive interferograms were calculated for each measurement campaign and summed to determine the total displacement magnitude. A more comprehensive description of radar interferometric methods is presented in Caduff et al.[35,36] The resulting displacements correspond to movements along the radar line of sight (Figure 1a). Displacements perpendicular to the view direction cannot be detected with this measuring system.

2.3 | Geophysics

An H-GPR survey was flown over the Furggwanghorn rock glacier in March 2013 to investigate bedrock depth and internal structures.[24] A 60 MHz GPR system was mounted directly under the helicopter and accurate positioning was obtained by differential GPS. Average flight height was 15–20 m. A total of 8100 profile metres was acquired in 16 approximately 450 m long lines, parallel to the flow direction of the rock glacier, and four approximately 340 m long lines perpendicular to it. Data processing was relatively standard, including a single-value-decomposition filter to remove coherent noise, an amplitude-based gain and suppression of incoherent noise. A constant radar velocity of 0.17 m ns^{-1} was used for migration and time-to-depth conversion.[26]

The main internal units of the rock glacier and the bedrock below were identified on the H-GPR sections by correlating reflection patterns in the subsurface and observations on aerial images and at the field site. Reflections from the active part of the rock glacier are characterised by high reflectivities and dipping reflection patterns, whereas the inactive part is more transparent on the GPR sections. The sharp transition between these zones corresponds to the main shear zone. The onset of reflections below the transparent zone marks the top of the bedrock. Details of the interpretation are found in Merz et al.[24]

2.4 | Cameras

Four cameras were used to monitor time-dependent surficial movements of the depressions in the vicinity of the root zone and of the rock glacier front. The cameras (Cannon EOS600) had a lens focal length of 18–55 mm and were installed inside weatherproof boxes overlooking the rock glacier. The positions and view direction of the cameras are given in Figure 1a (K1-K4). Each camera acquired four to six photographs every 24 hours.

2.5 | Inclinometers

Three automatic in-place segmental inclinometers, type SAAF (ShapeAccelArray-field, Measurand, Fredericton, NB, Canada), were installed in the rock glacier to measure displacements and detect potential shear horizons at depth. The first inclinometer was inserted in borehole F5 (24 m long, Figure 1a) in October 2010. The remaining two instruments were placed in 2011 in boreholes F6 and F7 (each 28 m long) in combination with thermistor chains. Details of the inclinometers are given in the Table S4. The data processing was carried out using the software SAAF_raw2data, version 3.21 from Measurand.[37]

2.6 | Differential GPS measurements

A GPS surveying system from Leica (C10/C15) was used to determine the position of single points at the boreholes and to map the area around the depressions in the root zone. The theoretical accuracy of the instrument in the horizontal and vertical directions (10 mm + 1 parts per million and 20 mm + 1 parts per million, respectively) could not be achieved without a mobile phone connection,[38] although this could be partially compensated for by measuring the points for a longer period and data post-processing using information from swipos-GIS/GEO (http://www.swisstopo.admin.ch), so that variations of less than 10 cm could be identified. The measurement error is considered acceptable, given the unevenness of the rock glacier surface.

2.7 | GPS stations

Five GPS stations were installed in July 2012 adjacent to boreholes F1, F2, F5 (on top of the weather station), F6 and F7. The GPS antennas were mounted on top of a conical plastic element, which was fixed on a steel mast on a concrete base (Figure S1a). Low-cost single frequency GPS receivers and antennas from u-blox (Thalwill, Switzerland) were used. The coordinates of all GPS stations are given in Table S5.

The GPS data were processed with Bernese GPS Software,[39] based on single-frequency differential carrier phase techniques. A permanent geodetic GPS reference station, operated by the Institute of Geodesy and Photogrammetry (ETH Zurich), was used as a reference for processing. The distance between the reference and the five GPS stations on the rock glacier is approximately 10 km.

Coordinates were estimated daily in static mode, so that one position was computed per day, with the GPS data covering 24 hours, representing mean positions over this period. An accuracy of 3 mm was obtained (empirical standard deviation, based on a regression line over several weeks) for the horizontal coordinates and 6 mm for the vertical coordinates. The displacements of the GPS stations were computed by substituting the initial coordinates from the coordinate time series, and the daily velocities were calculated using linear regression over a moving window of 8 days.

Two separate acceleration sensors were installed on each GPS mast to measure inclination in two orthogonal directions so that displacement of the plinth, upon which the GPS mast was mounted, could be calculated by using simple trigonometry. The rotation height was set equal to the mast height, although this may be an oversimplification because the plinth is not necessarily the rotating point of the system. The real rotation point is probably located further down, and depends on the diameter of the boulder on which the instrument is founded. This potentially leads to an error of a few centimetres in fixing the exact rotation point (Figure S1b). Nevertheless, meaningful results could still be obtained, based on this simplification.

Readings at the GPS station at borehole F5 were interrupted shortly after the commissioning until the beginning of January 2014. The GPS station at borehole F2 only functioned for about 3 months; these results have been omitted. No measurements were available from the GPS at borehole F6 after the beginning of 2013.

2.8 | Weather station

Precipitation, air temperature, humidity, snow depths, wind and radiation were measured at the weather station adjacent to borehole F5. The precipitation in liquid and frozen state was measured with a weighing rain gauge (Pluvio2 from OTT). Precipitation was recorded at 60 min intervals until July 10 2012 and thereafter at 5 min intervals, and summed daily. Snow depths were determined using an acoustic sensor (SR50A from Campbell). Details of the instruments are presented in Buchli et al.[21]).

2.9 | Ground temperature measurements

Ground temperature was measured in boreholes F1-F4 and F6/F7 using thermistors (type MEAS 44031, http://www.meas-spec.com) at different depths to 28 m.[21]

2.10 | Water content measurements

Water content in the rock glacier was measured from September 2011 to June 2015 using time-domain reflectometers (TDRs) installed at depths of 0.25, 0.5, 0.75 and 1.0 m within a trench, which was excavated and backfilled next to the weather station. Details are given in Zhou et al.[22]

3 | RESULTS

3.1 | Rock glacier surface deformation

The TLS results show large creep movements of several metres per year, increasing from the root zone down to the rock glacier front (Figure 2) for the years 2011–15. Surface displacements are divided into horizontal and vertical directions, for ease of interpretation. The horizontal displacements are shown as vectors, including direction and annual movements. The mid and northern parts of the rock glacier show the largest displacements, between 4 and 6 m y^{-1} and are moving mainly in a northwest direction. In comparison, the southern front lobe[24] and the slopes to

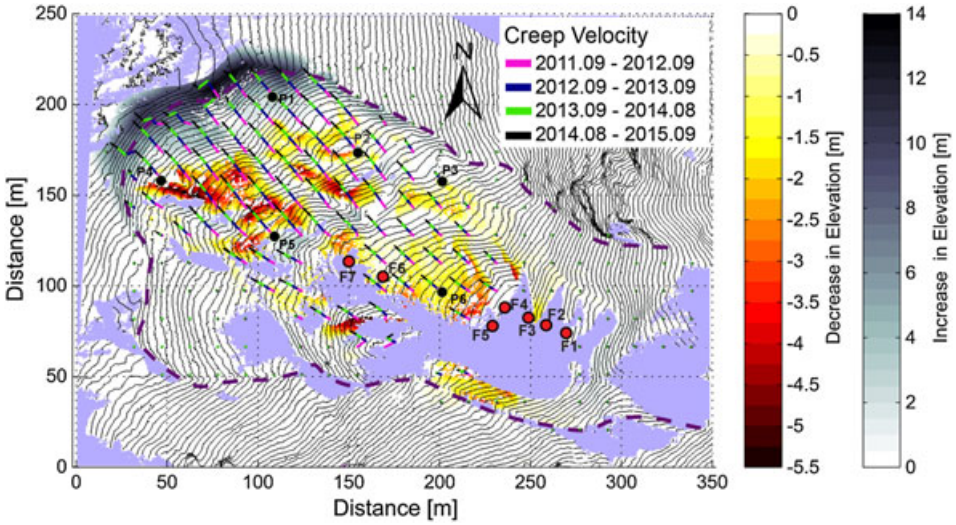

FIGURE 2 Map showing horizontal displacements (vectors), decrease in elevation of the rock glacier surface (red colours) and forward creep movements of the rock glacier as concluded from positive changes (gray colours) in surface elevation by using terrestrial laser scanning (TLS) measurements (September 2011 to September 2015). The vector lengths correspond to the net horizontal displacements over 1 y. Pink displacement vectors, derived from PIV analysis, indicate displacement between 2011 and 2012, whereas blue, green and black vectors represent displacements between 2012 and 2013, 2013 and 2014, and 2014 and 2015, respectively. Areas without data are coloured violet. The positions of boreholes F1-F7 are indicated as red dots. Contour interval 1.5 m. Creep velocities were derived from comparison of hillshade models based on multi-temporal TLS measurements (2001–2015). The creep velocities for six selected points (P1-P6: black dots) are summarised in Figure 3 [Colour figure can be viewed at wileyonlinelibrary.com]

the north and east of the depressions seem to have been inactive during this period. This forced successive lobes (2 and 3) to spread to the northwest on a curvilinear path, while a new lobe (e4) advanced over lobes 1–3. The remaining displacements in the area around the depressions could not be determined, due to lack of data.

A compilation of horizontal creep velocities for six selected points (Figure 2) is given in Figure 3, with displacements ranging from 2.6 m during the period 2013/14 (P3) up to 7 m (P4) in the period 2014/15. Figure 3 illustrates that the local displacements did not increase at a constant rate but fluctuated substantially over the measuring period. Initially, P1, P2 and P5 were creeping at the same rate, although creep velocity was universally lower during 2013/14 than before. Subsequently, P4 accelerated and P1 decelerated.

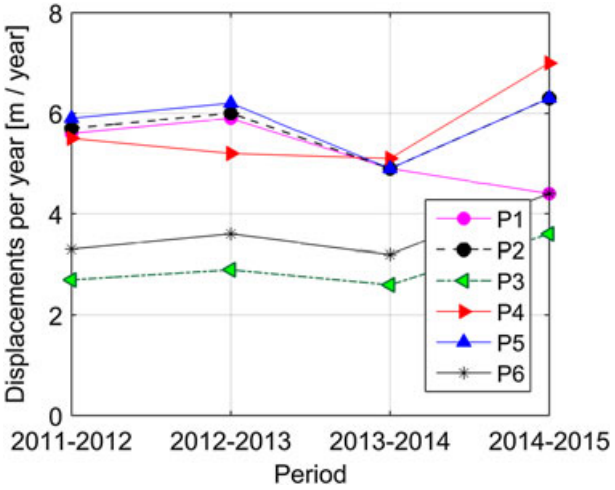

FIGURE 3 Calculated annual creep rates for six single points at the surface, shown as black dots in Figure 2, based on TLS measurements (2011–12, 2012–13, 2013–14, 2014–15) [Colour figure can be viewed at wileyonlinelibrary.com]

Vertical changes in the range of metres were determined by comparing the *z* coordinates of the measured surface for 2011 and 2015, while neglecting any settlement or heave smaller than 5 cm. Total surface subsidence of up to 5.5 m occurred locally over the 5 year period of measurement, particularly in the main flow zone (Figure 2). In contrast, total displacements in the upper part of the rock glacier ranged from 0 to 1.5 m. Positive changes in height can be due to an advancing rock glacier front or single boulders moving on the rock glacier surface. Rock glacier creep in the northwest direction at the front, and some small areas in the main flow zone, exhibited positive changes in elevation.

The displacements from the fixed GPS stations at boreholes F1, F5, F6 and F7 were plotted as a function of time in the horizontal and vertical directions (Figure 4a, b, respectively). Figure 4c shows the displacement in plane view (from east to west and from south to north). The device at borehole F5 failed for several months, shortly after initiation. The creep of each of the four GPS stations follows a consistent direction and almost no lateral movements were detected (Figure 4c). In most cases, lateral peaks are not attributed to a change in the movement direction because the GPS mast tilted and rotated around a point at an unknown depth (Figure S1b). Hence, the displacement calculated at the foot of the GPS mast may not always correspond exactly to the real displacements.

The GPS located at borehole F1 showed horizontal and vertical displacements of nearly 1 and 0.4 m, respectively, from July 2012 to June 2015, occurring more or less at a constant rate. The GPS sensor mounted on the weather station (F5) indicates linear horizontal and vertical displacements up to 8 and 4.5 m, respectively, during the measuring period. The step change on August 2 2014 (point A) was due to resetting the inclined mast of the GPS station back to vertical. The largest movements were measured at borehole F7, with ~15 m in a horizontal direction and nearly 6 m vertical, which is repeated at borehole F6 until December 2012. This suggests significant translational

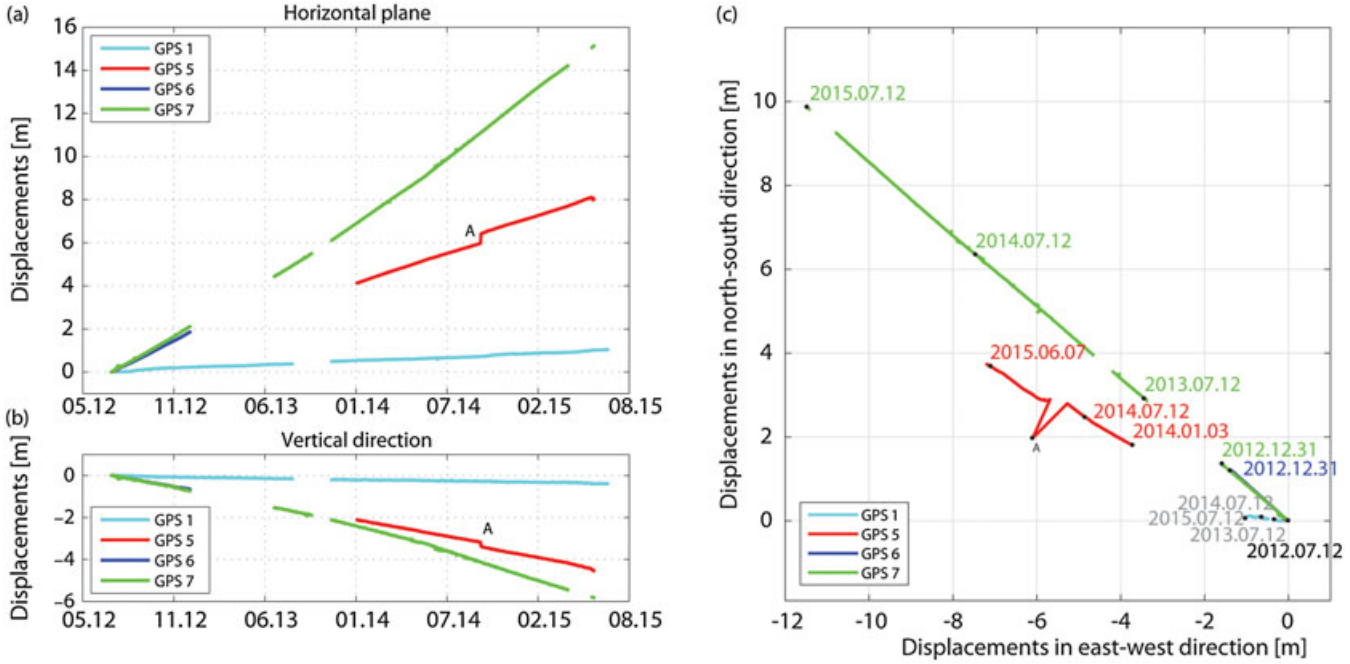

FIGURE 4 GPS displacements as a function of time, separated in a horizontal plane (a) and the vertical direction (b). (c) Graph summarising the displacements in north–south and east–west orientations. The GPS data for borehole F6, which stop in January 2013, are mostly overlain by data for borehole F7. Point A marks the point when the GPS mast for F5 was reset to the vertical [Colour figure can be viewed at wileyonlinelibrary.com]

movements took place between the two boreholes. F7 appears to have accelerated gradually from around 4.5 m y^{-1} in 2012 to 5.8 m y^{-1} in 2015. Table 1 summarises the annual velocities for all GPS stations in the plane and the resultant 3-D directions. Borehole F1 showed small west northwest movements, while borehole F5 moved more to the northwest. Boreholes F6 and F7 were both northwest oriented. The main flow direction changed to the orographic right.

3.2 | Cross-sectional internal structure

The context between the four active lobes (lobes 1–4: Figure 5), which were determined first by Merz et al.,[24] the surface deformations and the internal shear zones are illustrated with four cross sections through the rock glacier in Figure 6. Cross sections C_{1ab} and C_{2ab} run transversally, whereas C_{1cd} and C_{2cd} extend in the flow direction from the root zone down to the rock glacier front. Four additional cross sections are presented in Figures S3 and S4.

TABLE 1 GPS velocity (m y^{-1}), projected to the foot point of the station, calculated for 1 y

		2012	2013	2014	2015
F1	2D	0.46[a]	0.32	0.31	0.38[a]
	3D	0.50[a]	0.34	0.33	0.41[a]
F5	2D	2.79[a]	2.79[a]	2.93	2.30[a]
	3D	3.14[a]	3.14[a]	3.37	2.91[a]
F6	2D	3.91[a]	—	—	—
	3D	4.16[a]	—	—	—
F7	2D	4.45[a]	4.77	5.76	5.81[a]
	3D	4.71[a]	5.06	6.22	6.30[a]

[a]Values interpolated/extrapolated.

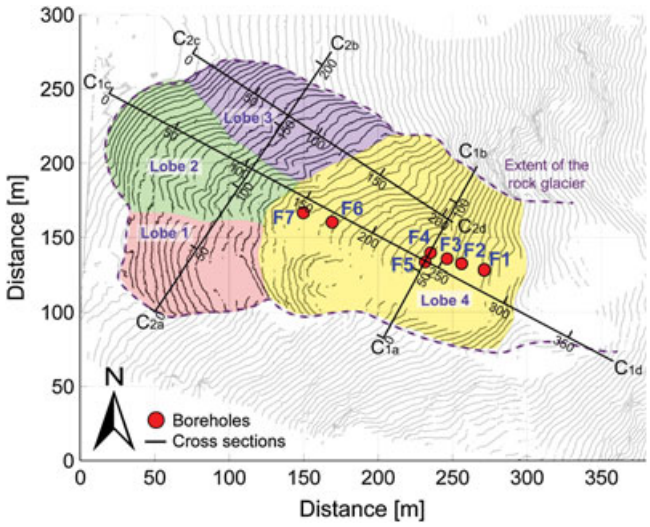

FIGURE 5 Plan view of the position of vertical cross sections shown in Figure 6. The coloured sections mark the four lobes in the plane direction. Contour interval 2.5 m. Boreholes F1-F7 are indicated as red dots [Colour figure can be viewed at wileyonlinelibrary.com]

3.2.1 | Cross sections C_1

Cross section C_{1cd} shows clear evidence of forward movements in the front part, whereas subsidence is visible at various locations along the profile (Figure 6a). The shear zone in the main flow zone (pink) is deeper and almost parallel to the surface. The generations of more recent lobes can be determined above this, mainly with lobe 2 (green) in the front and lobe 4 (yellow) in the upper part of the rock glacier. latter is delineated at a depth of more than 10 m in the transverse section.

Uniquely, an ongoing failure mechanism was identified in the depression area by combining the shear zone measured with inclinometer F5 with the base of lobe 4 and extending it upslope through

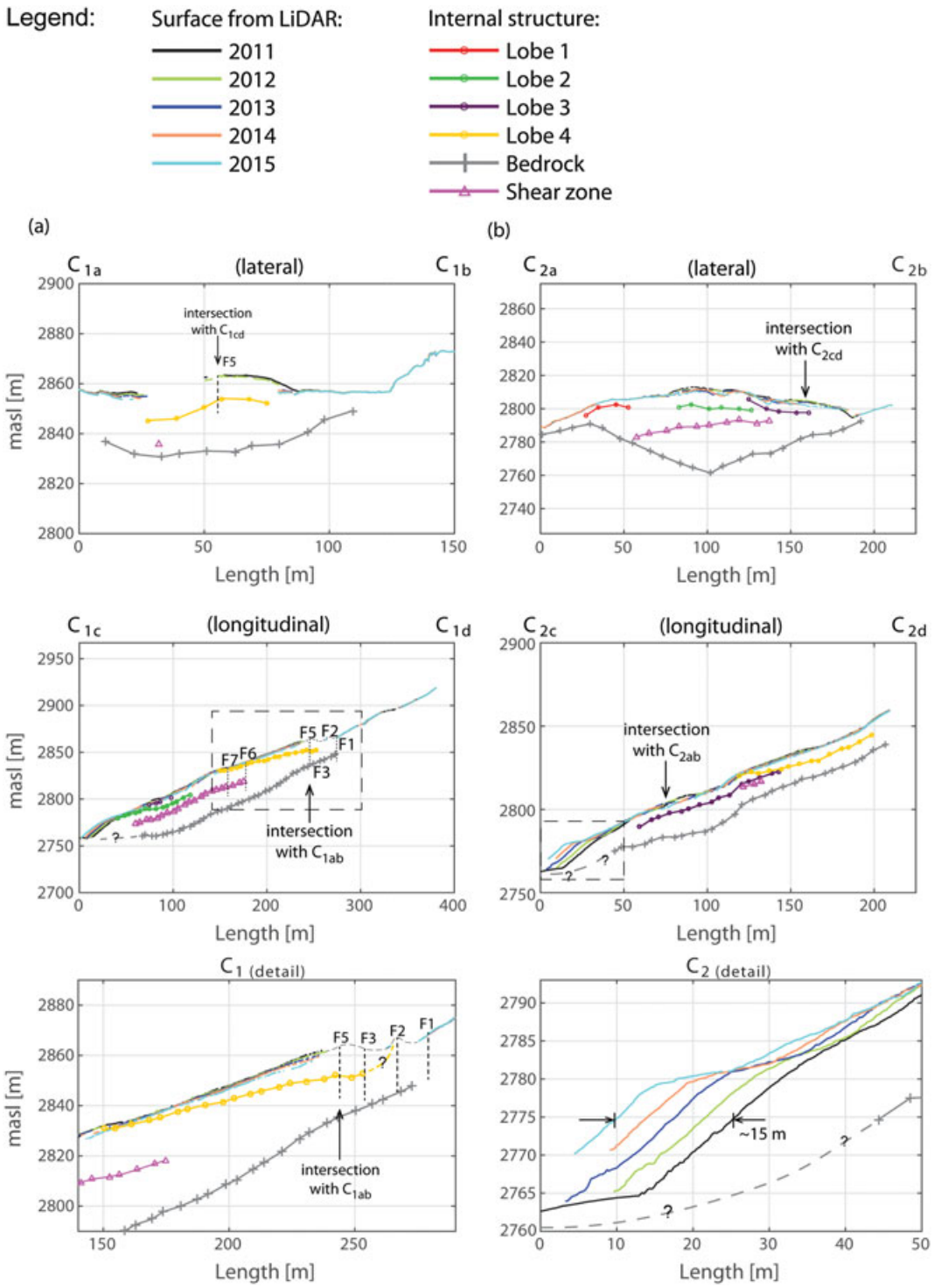

FIGURE 6 Vertical cross sections C_{1ab}, C_{1cd}, C_{2ab} and C_{2cd} through the rock glacier. The alignment of the cross sections is given in Figure 5. Dotted lines complete any surface that could not be seen with the TLS instruments and the question marks indicate unknown or ambiguous data. Enlargements of the bedrock, lobe differentiation and shear zone are given in $C_{1\ (detail)}$ and of the rock glacier front in $C_{2\ (detail)}$ (see dashed rectangles in C_{1c} and C_{2c}) [Colour figure can be viewed at wileyonlinelibrary.com]

borehole F3 to daylight near borehole F2 (Figure 6a, $C_{1\ (Detail)}$). Direct field observation of the rotation toward the root of the F3 plinth supports this hypothesis (Figure S1).

3.2.2 | Cross sections C_2

The northern part is the most active, with considerable surface changes and movements both downslope and perpendicular to the viewing direction (C_{2ab}: Figure 6b). The resultant displacement vector is to the northwest (Figures 2 and 4).

The internal structure is dominated by lobe 3 (magenta), which is overlain by lobe 4 (yellow) to the east. The ancient shear zone (pink), located in the older deposits below lobes 1, 2 and 3, was more identifiable transversally than longitudinally (length = 125–135 m), nearly matching the depth of lobe 3. Depth to bedrock follows a nearly v-shaped bedrock profile and is approximately 20 m

below the rock glacier surface along the longitudinal section (Figure 6b).

The advance of the front was at a steady annual rate accumulating to nearly 15 m during the observation period (see $C_{2\ (detail)}$ Figure 6b). Negligible settlement occurred in the south-west (C_{2a}), whereas a decrease in elevation of about 1.5 m could be detected in the northeast (C_{2b}). Similarly, settlement occurred upslope toward C_{2d}.

3.3 | Rock glacier front

Most of the front slopes of the Furggwanghorn rock glacier exceed 40°, with elevations of about 15 m (Figure 6b, $C_{2\ (detail)}$). Apart from large translational movements, several local instabilities were observed on the northwest front of the rock glacier, which ranged from toppling of boulders to local slope failure. These were often combined with water outflow in mid- to late summer.

Photographs taken from camera K4 (Figure 1a) illustrate the advance of the rock glacier front from August 2013 to September 2015, showing significant movements at the foot (A) and crest (B) of the front slope (Figure 7). A block visible at C was later buried by the advancing rock glacier.

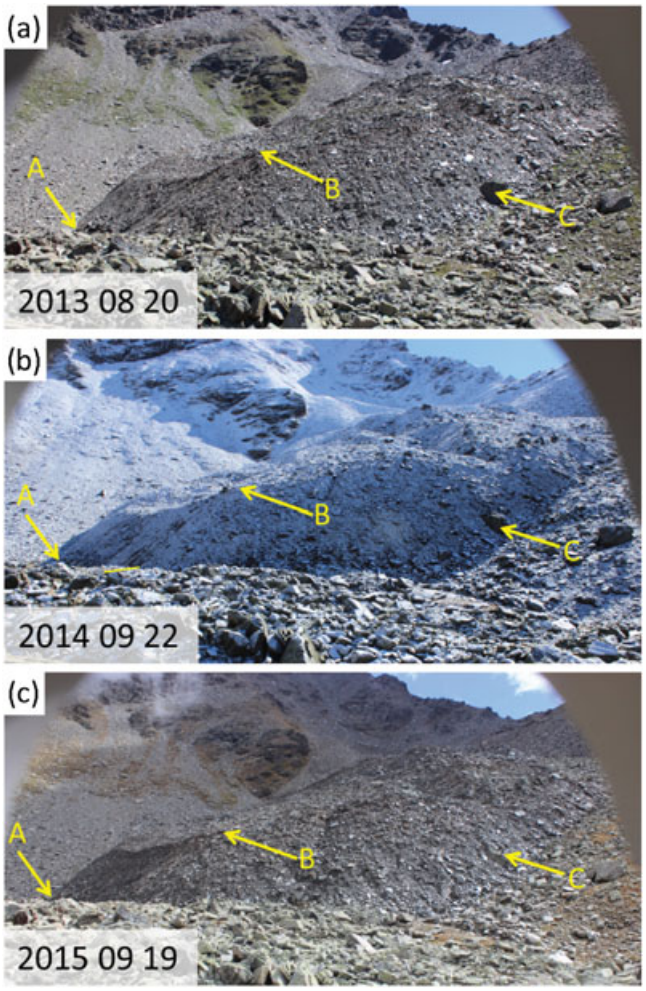

FIGURE 7 Annual photographs of the rock glacier front, taken between August 20, 2013 and September 19, 2015 by camera K4 [Colour figure can be viewed at wileyonlinelibrary.com]

Photographs from cameras K3 and K4 repeatedly showed water outflow, especially at midheight at the rock glacier front between A and B (Figure 7). Different front slope responses were attributed to resulting erosion and investigated through the radar measurements made over roughly 24-hour periods in summer and autumn (Table S2). The visual observations were confirmed and movements were quantified for each radar measurement campaign (Figure 8).

Displacements in centimeters of the rock glacier toward the radar were normalized to the same contour scale over 24 hours in the rainbow color-coded areas (Figure 1a). Uncolored areas either represent displacements of less than 0.2 cm d^{-1} or were out of sight of the radar position (ie, no information was available). The minimum and maximum air temperatures during the measuring period are given to estimate whether water outflow at the front was likely.

More displacements occurred locally during the summer (Figure 8a–d) than during the autumn campaigns (Figure 8e–i), indicating variable underlying downslope creep rates at both times. The summer campaign in July (Figure 8a) also revealed a different response from the others, when water flow was likely from late snowmelt. These outflows stimulated local slope instabilities at midheight, leading to debris accumulation at the base of the slope. Displacements of up to 6 cm d^{-1} were mainly restricted to local zones at the front, with greater displacements at the bottom than at the top.

The smallest displacements, with a range of less than 1 cm, were measured at the rock glacier boundary, where it meets the underlying terrain. Generally, displacements were greater at the top of the front slope than at the bottom (Figure 8e–i), indicating slight steepening during the measurement period.

3.4 | Movements and thaw lakes in the depression zone between boreholes F1 and F4

Two clearly visible depressions oriented north–south were extending in the upper part of the rock glacier, almost across the entire width, and reached several metres deep in cross section. Figure 9a–d shows surface changes in the upper part of the rock glacier through a sequence of photographs taken from the same camera position K1 (Figure 1) between autumn 2012 and summer 2015. Three prominent points were chosen for comparison: (1) borehole F7; (2) the weather station (F5); and (3) point A, a boulder uphill of the depression below F1. It is clear that the borehole (F7) and the weather station (F5) were creeping downslope over the observation period, whereas little displacement occurred at point A.

A small circular depression, filled with water, is discernible in Figure 9b (September 2014) and was observed in summer 2013 and 2014. Water was visible repeatedly during the snowmelt period and remained dammed for several weeks until a drainage path developed. The timescales were derived from photographs, although field records show evidence of a similar occurrence before 2013.

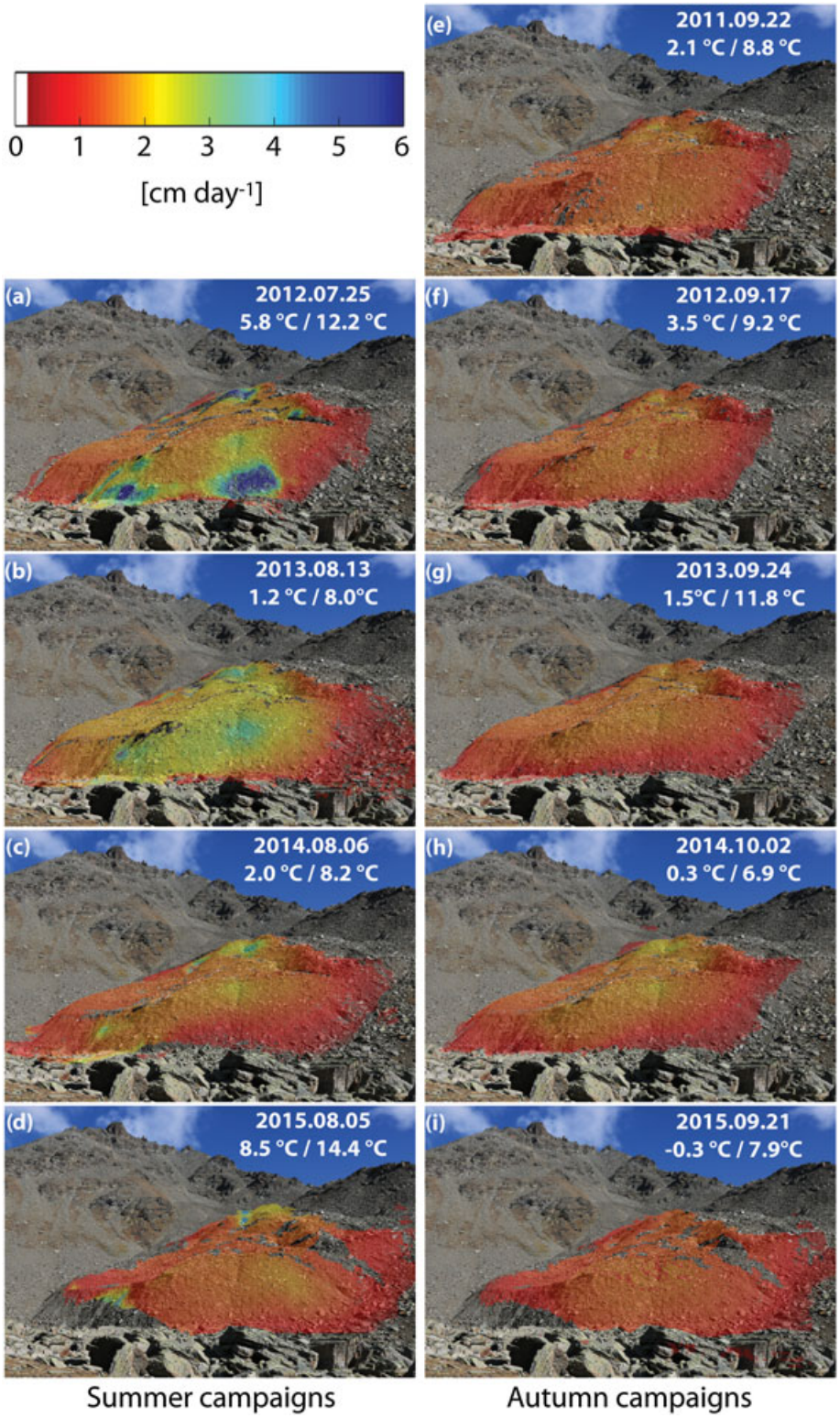

FIGURE 8 Creep velocities per day based on radar measurements on the rock glacier front during seven measurement periods. The given temperatures correspond to the minimum and maximum air temperature during the measurement campaign. Noncoloured areas: displacements of less than 0.2 cm d^{-1}/out of sight [Colour figure can be viewed at wileyonlinelibrary.com]

3.5 | Internal creep behaviour (shear zones)

Each of the three segmental inclinometers (F5, F6 and F7) shows only one distinctive shear zone, with almost no downslope creep detected above it. The inclinometer results for the three boreholes are shown in Figure 10 as a function of depth (24 m in F5, 28 m in F6 and F7) for 7.5, 10 and 5.3 months, respectively.[37]

The main shear deformations extend over 1–3 m (2–6 segments), which were detected in boreholes F5, F6 and F7 at depths of around 15, 20 and 18 m, respectively. The average creep velocity in the shear

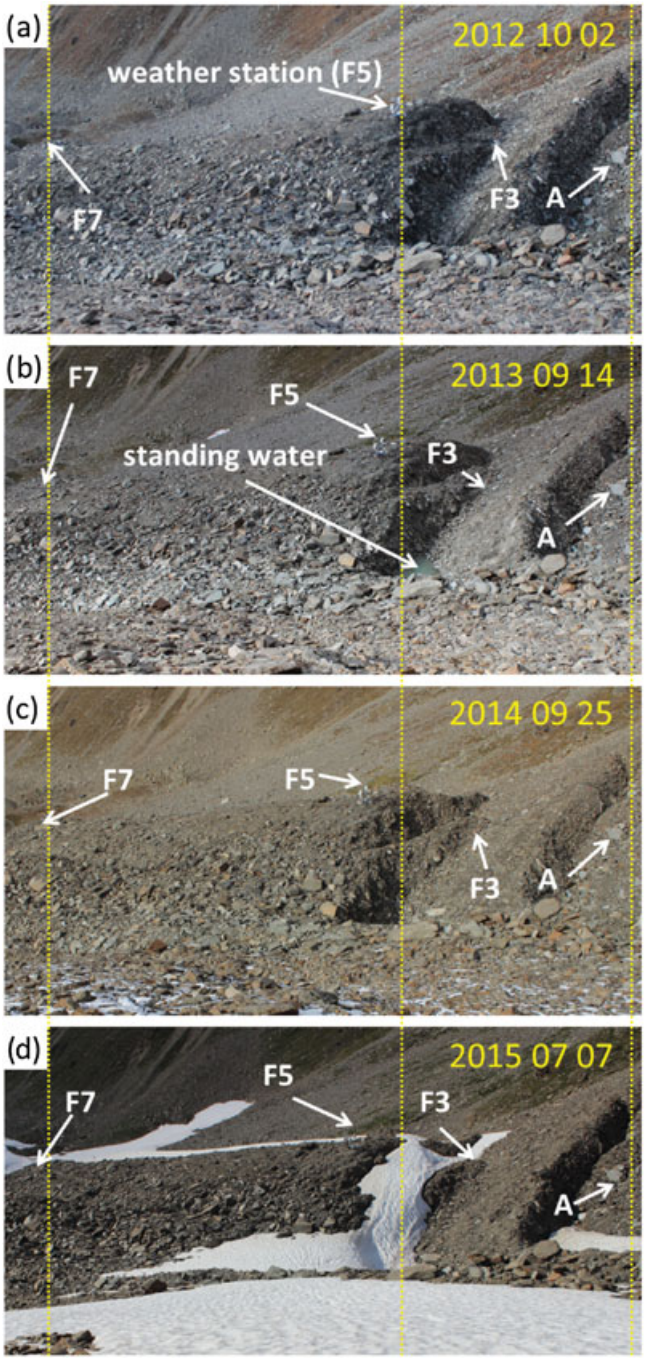

FIGURE 9 Annual photographs of the depression zones, taken between October 2, 2012 and July 7, 2015 by camera K1 [Colour figure can be viewed at wileyonlinelibrary.com]

zone was about 1 cm d^{-1} for inclinometers F6 and F7, twice as large as that for F5.

The inclinometer proved more robust than predicted given the inextensible joints between each 0.5 m long inclinometer segment, as the segment chain was "pulled" through the sand packing inside the polyethylene tube, remaining intact for up to 10 months. A maximal shear displacement of nearly 3 m could be measured in borehole F6, accompanied by apparent loss of height (Figure 10), which was compensated for either partially or fully by the ongoing settlement of the rock glacier surface (Figure 2).

Unexpectedly, the downslope displacements of inclinometers F5 and F6 at the surface were slightly lower than the maximum displacements at the shear zone, contrary to all reported past data (eg, [17]). This is only explainable physically if backward rotation occurred above the shear zone, instead of pure translational movements. This was confirmed by further field observations on the ground next to the corresponding inclinometers, where the plinth at borehole F3 rotated eastwards.

3.6 | Comparison between creep velocities with hydrological and thermal measurements

Possible connections between the creep behaviour, the hydrological and the thermal measurements are visible in Figure 11. Air temperature is plotted in Figure 11 with precipitation, snow height and borehole temperature close to the sherar zone. Furthermore, measurements of volumetric water content (TDR) obtained from a 1m deep test pit next to borehole F5 and the inclinatometer and GPS velocities are also plotted. The TDR data were measured at depths of 0.25, 0.5, 0.75 and 1.0 m beginning in September 2011.

Velocities were calculated over a 24-hour period, both from the inclinometer and from the GPS stations. The GPS displacements are a best estimate of the position and are therefore associated with some uncertainty (Table 2); hence, the standard deviation is given for the GPS velocities directly in color in the figure behind the black lines. The reason for the prominent peaks at GPS F7 between July and October 2014 cannot be explained based on the available data. Several simple flow calculations, with variable infiltration times, were carried out to find a statistically significant relationship between the marked velocity peaks and previous precipitation events. No time-delayed connection was found that would fit most of the peaks of one single instrument regularly, contrary to findings by Wirz et al.[40] for another rock glacier under similar conditions in the Swiss Alps. Therefore, it can be concluded that the flow paths on the Furggwanghorn rock glacier differ significantly and are not easy to describe mathematically.

For simplification, the inclinometer velocities presented for all three instruments correspond to the velocity at the surface. This is reasonable, because the inclinometer profiles show a nearly vertical profile above the shear zone (Figure 10).

Boreholes F6 and F7 contained an inclinometer and thermistors, allowing displacements and temperatures to be compared directly (Figure 11). The ground temperature for F6 and F7 is given for depths of 20.75 and 18.25 m, respectively. No thermistors were installed in borehole F5, so the corresponding values from borehole F4 (around 10 m from borehole F5), which exhibit similar behaviour, are presented.

4 | DISCUSSION

4.1 | Kinematic behaviour of the rock glacier

The entire surface of this degrading rock glacier has become more uneven since 2000, with four lobes clearly visible.[24] This can be

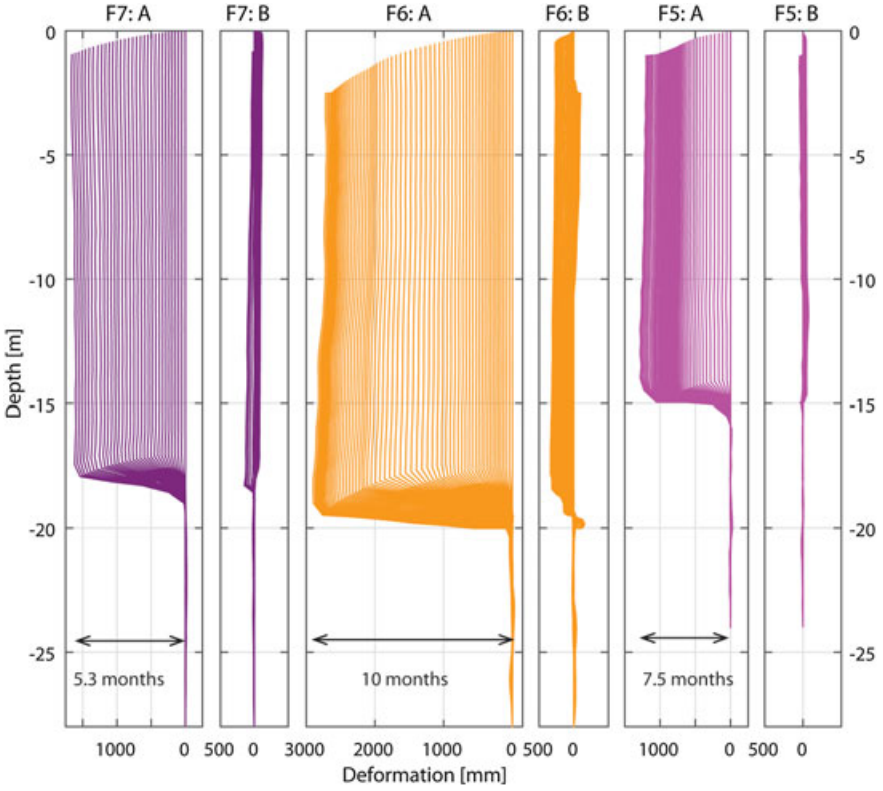

FIGURE 10 Inclinometer displacements (plotted with a time interval of 5 d) measured from boreholes F5, F6 and F7. The total inclinometer displacements are separated into a main flow direction A, and a perpendicular direction B.[37] Borehole locations and directions A and B are given in Figure 1 [Colour figure can be viewed at wileyonlinelibrary.com]

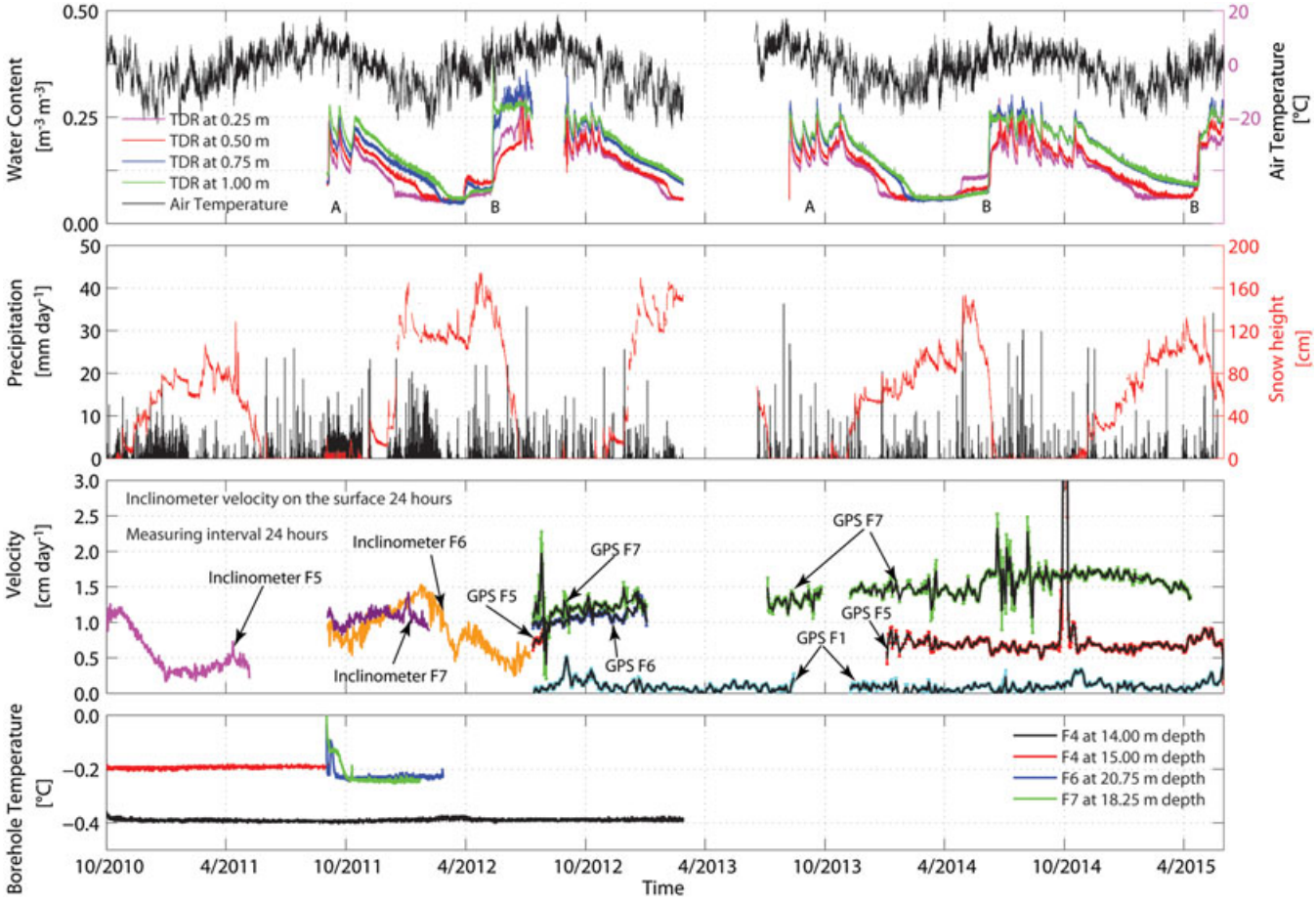

FIGURE 11 Time series of air temperature, water content, precipitation, snow thickness, ground temperature and creep velocities determined from GPS measurements and inclinometers. The GPS-derived creep velocities are given with black lines; a coloured background indicates the corresponding standard deviation [Colour figure can be viewed at wileyonlinelibrary.com]

TABLE 2 GPS velocity over the entire measuring period with standard deviation and the azimuth of the displacements calculated on the foot point (mean values)

Station	East (m y^{-1})	North (m y^{-1})	Height (m y^{-1})	
F1	−0.317 ± 0.001	0.041 ± 0.000	−0.117 ± 0.000	
F2	−0.201 ± 0.045	−0.056 ± 0.053	−0.171 ± 0.107	
F5	−2.532 ± 0.010	1.338 ± 0.003	−1.624 ± 0.006	
F6	−2.932 ± 0.006	2.601 ± 0.005	−1.416 ± 0.006	
F7	−3.972 ± 0.009	3.404 ± 0.008	−2.004 ± 0.008	
Station	**2D (m y^{-1})**	**3D (m y^{-1})**	**Azimuth (°)**	**Slope (°)**
F1	0.320 ± 278.7	20.7 ± 0.001	278.7	20.7
F2	0.208 ± 254.4	39.4 ± 0.076	254.4	39.4
F5	2.864 ± 297.6	27.9 ± 0.009	297.6	27.9
F6	3.920 ± 311.6	19.9 ± 0.005	311.6	19.9
F7	5.231 ± 310.5	20.0 ± 0.008	310.5	20.0

attributed to creep-dominated effects that relate to lobe development and melting of ice that leads to settlement. The main kinematic findings can be related to the four areas defined according to their geomorphology (Figure 1b) and summarised here.

a. Root zone: displacement rates of several centimetres per year were observed in this zone without significant changes to the surficial state.
b. Depression zone: significant surface change since the Roer et al.[25] study include development of depressions, perpendicular to the flow direction to a depth of more than 10 m, which were barely visible in 1993. Buchli et al.[21] measured the permafrost ground temperatures down to 25 m in four boreholes as being close to 0°C. The ground properties were extremely heterogeneous, even over distances of a few metres.[21,41] The visible changes taking place at the surface may therefore be a consequence of creep along defined shear zones as well as volume loss due to reduction in ice content, accelerated by the flow of meltwater streams along preferential paths inside the rock glacier[22] that affect degradation progresses.
c. Main flow zone: translational movement rates of more than 5 m y^{-1} were measured at different places in this zone.
d. Front zone: Roer et al.[25] reported mean annual creep velocities at the rock glacier front of 1.55 m y^{-1} for the period 1975–2001, based on terrestrial and aerial photogrammetry. Velocities have now increased approximately threefold.

4.1.1 | Surface structure: lobes

Figure 12 depicts the four different lobes (Figure 12a) and compares them with the velocity distributions of the rock glacier surface (Figure 12b), which show lateral spreading and downslope movement at the front. The overriding deformations are dictated currently by a combination of gravity-driven flow, topography of the past lobes and the creep-susceptibility of the ice phase in the deforming mass and are neither congruent with the four detected lobes (Figure 12a) nor congruent with the geomorphological zones defined in Figure 1.

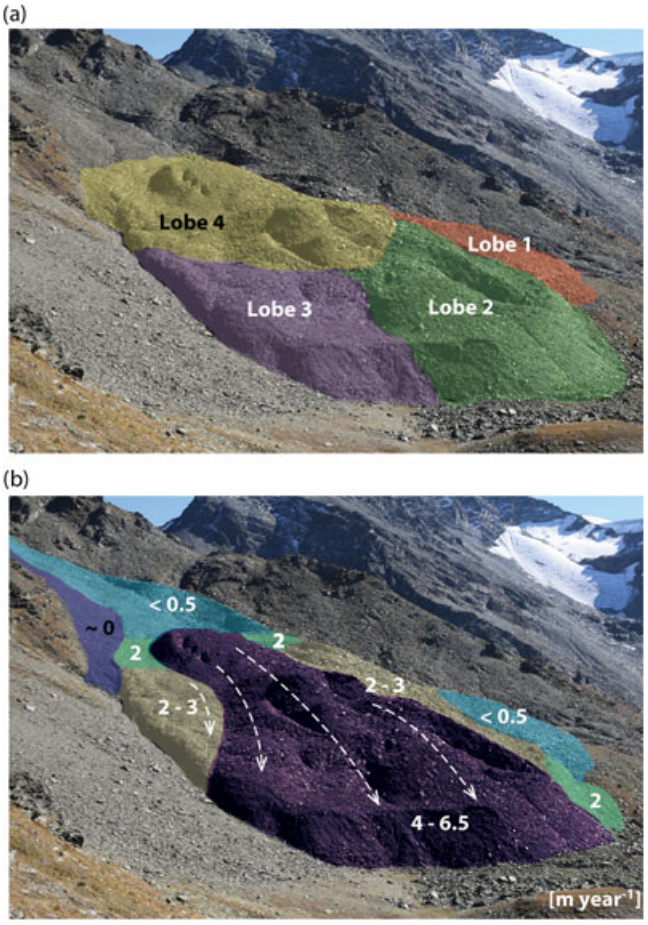

FIGURE 12 Photographs showing (a) the four lobes of the Furggwanghorn rock glacier and (b) and the surface displacements (in m y^{-1}) [Colour figure can be viewed at wileyonlinelibrary.com]

TLS and radar measurements demonstrate that the southern lobe 1 of the rock glacier front shows little or no deformation during the observation period (Figures 6–8 and Supporting Information). This forced successive lobes (2 and 3) to spread to the northwest on a curvilinear path, while a younger lobe (4) advanced over lobes 1–3.

The inclination of the surface shown in Figure 13 indicates a change in slope where the shear zones crop out at the surface. It can be inferred that lobes 2 and 4 can be divided into at least two different sublobes (Figure 13; $L2_A$, $L2_B$, $L4_A$, $L4_B$). It is highly probable that earlier movements occurred along these shear surfaces, as deduced from the H-GPR profiles.[24]

4.1.2 | Internal structure: shear zones and failure mechanisms

The four lobes geomorphologically express the underlying shear surfaces (eg, [42,43]). At least three main active failure mechanisms, defined as a kinematically admissible series of shear displacements along consecutive elements where the applied actions exceed the maximum shear resistance, can be detected along various cross sections in the current state of the rock glacier (Figure 13; L2, $L4_A$ and $L4_B$). Ground movements above the shear surface could be rotational, translational or a combination of these.

The internal 3-D structure and movements are presented in a simplified schematic model (Figure 13), which extends approximately

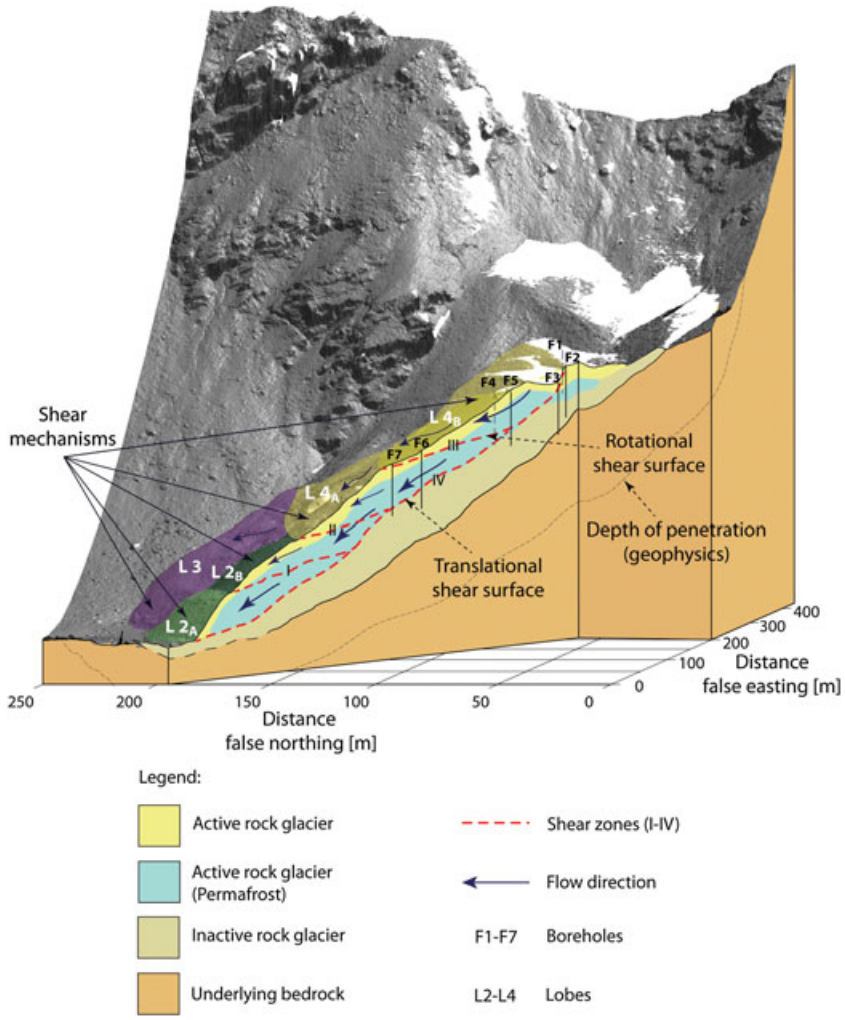

FIGURE 13 3-D block diagram showing a cross section through the rock glacier along boreholes F1-F7, shear zones and possible failure mechanisms [Colour figure can be viewed at wileyonlinelibrary.com]

along the axis of boreholes F1-F7. The model is limited to the penetration depth of the GPR-signal (dashed lines) and contains information about both the composition of the ground and possible failure surface(s). Three main layers are identified: the active (permafrost body and active layer) and inactive (above-zero temperature) parts of the rock glacier body and the underlying bedrock.

Four main overlapping shear zones (I-IV) are located along boreholes F1-F7 (Figure 13). The upper shear zones I, II and III start at the surface, extend diagonally uphill and end in shear zone IV, which runs roughly parallel to the surface.

Shear zone I is probably inactive, although this assumption is difficult to prove, since no inclinometers were installed in this area. Consequently, lobe 2 is thought to be moving en bloc along shear zone IV.

Based on the inclinometer measurements from boreholes F6 and F7, it is considered that the lower part of lobe 4 ($L4_A$) was creeping along shear zone II at the time of observation. This failure mechanism shows both translational and rotational movements, because of the slightly rotational behaviour of inclinometer F6 (Figures 10 and 14a).

Comparison of the TLS measurements along borehole axes F1-F7 for different years (Figure 6, C_{2cd}) shows that the ground surface above the outcrop of shear zone II moved horizontally. This area also moved vertically because of the inclined bedrock topography and volume loss due to ice melt. Because the underlying lobe 2 also moved, it is difficult to estimate how lobes 2 and 4 moved relative to each other, which supports the hypothesis that gravity-driven flow had become dominant.

Although geophysical investigations had indicated that borehole F6 crossed shear zone III just below the surface,[24] this could not be confirmed from inclinometer measurements. A possible explanation is that the upper shear zone (III) was still active but showed insignificant relative displacements during the inclinometer monitoring period because a deeper shear zone (IV) became dominant. It is assumed that the material transport is out of mass balance, related to the supply of weathered material from surrounding rock faces and therefore the pressure required for creep movements in shear zone III may not exist.

Lobe 4_B, which moved along shear zone III, demonstrated both translational and rotational movement. The inclinometer data for borehole F5 imply rotational behaviour, as for borehole F6 (Figure 10). This can be confirmed by field observations as the two depressions have deepened further since borehole F2 was drilled on the top of a ridge between them in autumn 2010, while borehole F3 was located in a depression (Figure 14a). The ground under the downslope side of the concrete plinth (F2) started to erode in 2012, leading to increasing inclination and sliding in 2013, with subsequent partial loss of thermistor data. At the same time, the plinth at borehole F3 sank into the ground and rotated upslope toward the east, while plinth F4 settled and translated downslope. Based on these visual observations and in situ measurements, it is strongly suspected that the upper part of lobe

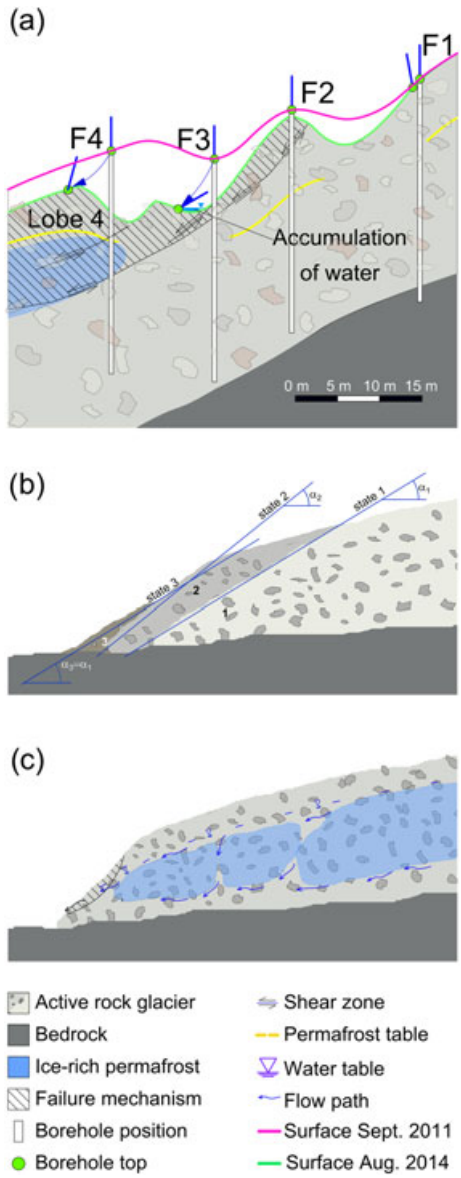

FIGURE 14 Schematic cross section through the rock glacier along boreholes F1-F4 for 2011 and 2014, with the borehole inclination for the two times given by blue lines (a), and through the front slope for the failure mechanisms due to underlying creep (b) and due to water flow (c) [Colour figure can be viewed at wileyonlinelibrary.com]

4 ($L4_B$), which is completely embedded in $L4_A$, rotated around the area of the weather station, instead of moving translationally, as observed further downslope.

The transition between the subzero, ice-rich zone and the zone with less or no ice[24] corresponded well with shear zone IV, which began at borehole F3 and ended at the rock glacier front. The thickness of the shear zone was about 2–3 m, based on inclinometer measurements in boreholes F6 and F7 (Figure 10). It is supposed that shear zones III and IV merged downhill of borehole F5 (Figure 13), since a single shear zone was shown in the inclinometer results (Figure 10).

The nearly straight inclinometer profiles above the shear zone (Figure 10) for all three inclinometers imply that creep was mostly limited to the shear zones, similar to findings from the Murtèl-Corvatsch and the Pontresina Schafberg rock glaciers.[17] Inclinometer results from Lazaun[18] also show an extended shear zone several metres thick.

The development of the main shear zone IV must relate to the corresponding ice content, since core samples extracted from borehole F7 and information from drilling other boreholes showed no clear change in the soil fabric extracted at these depths, which could indicate a zone with reduced shear strength,[27,41] as implied at Murtel-Corvatsch.[17] Arenson and Springman[13] showed that the amount of ice has a major influence on total shear resistance, which can be calculated after the Mohr-Coulomb model.[44]

The additional shear resistance in the ice-rich zone,[45] even though it was relatively "warm" at about −0.2°C,[21] forced shearing to develop at the transition zone with less ice. Since the effective stress σ' and therefore the shear resistance τ in unfrozen granular soils increases with depth,[46] shearing is unlikely to occur in deeper regions.

4.1.3 | Changes in topography at the depressions

Surface deformations in the area between boreholes F1 and F4 are presented in relation to the subsurface failure mechanisms in Figure 14a. By drawing the depth of the shear zone in borehole F5 (near F4) and the depression south of borehole F3 to scale, the most likely conclusion is that the two points are connected by a curve, which reaches the rock glacier surface at the original position of borehole F2. It is assumed that the ice content within the shear zone is lower than in the zone above, and therefore permeability is higher relative to the soil above.[47] Therefore, it can be postulated that the outflow of the accumulated meltwater within the depression next to borehole F3 is probably directly connected to this shear zone (Figure 14a).

A longitudinal surface profile along boreholes F1-F4 and F5 respectively, mapped in September 2011 with a hand-held GPS (Figure 14a, pink), was surveyed again in August 2014 (green). The positions of the boreholes during drilling in 2010 are also shown. Settlement occurred in the depressions, one of which has bifurcated, and significant lateral movement occurred at boreholes F3 and F4/F5. The rotation of the borehole can also be illustrated by indications of the borehole axes (vertical line on top of the boreholes) at the time of the drilling, and 3 years later (inclined blue lines). The difference in creep behaviour between boreholes F1 and F4/F5 is notable. The movements at borehole F1 (roughly 0.3 m y^{-1}) were driven by the deepening depression between F1 and F2, while boreholes F4/F5 demonstrated horizontal displacements of about 1.7 m y^{-1} and settlements of the same order. The top edge of borehole F2 could not be identified after 2014, because there was local failure and the rock debris sheared downslope (Figure 14a).

The inclinometer in borehole F5 operated for 7.5 months until displacements in the shear zone led to instrument failure, while the thermistor cables in borehole F4 nearby ceased functioning 12 months after installation. However, it is postulated that the critical rotational shear zone crops out just downslope of borehole F3, since the axis of the GPS pillar rotated almost 60° to the east and the thermistor cables in the borehole had not sheared at all during the observation period (Figure 14a).

4.1.4 | Changes of the geometry of the rock glacier front

Relatively large daily movements occurred at the rock glacier front, which varied seasonally, as seen from the radar results (Figure 8). The front remained stable for most of the time because of dilatancy, cohesion derived from ice or from suction due to partial saturation near water outflows. Nevertheless, two macro-failure mechanisms can be differentiated (Springman et al[19]), one driven year round by creep (Figure 8e-i) and the other periodically by hydrological processes (Figure 8a-d).

a. Figure 8 shows greater creep deformation at the top (yellow) of the rock glacier front than at the bottom (red), which is redrawn in cross section as states 1 and 2 with peak angle α_2 in Figure 14b. The creep caused the front slope angle α_1 to increase (from a stable state 1) to a maximum of α_2 at state 2 (due to effects that contribute to apparent or temporary cohesion) before renewed local shearing reduced it to α_1 (state 3), although state 3 was not observed during the radar measurements. These measurements focus on the daily changes and not on a specific state of the surface at a certain time, in contrast to the TLS observations.
b. Figure 8a and b indicate greater local movements around specific points on the front face, which can vary from year to year (eg, at the foot of the slope [blue] in 2012 and midslope [green] in 2013). This hints toward hydrologically induced failure, whereby water can flow on the top, below and through the permafrost (Figure 14c). This raises local pore water pressures and reduces effective stresses on a steep slope, causing erosion and local failure to occur. Failure is manifested in displacements represented in Figure 8a and b, with debris accumulating either locally on the slope or at the toe, and displacements were less dominant in the following 2 years (Figure 8c, d). This was probably due to timing of the measurements and the snowmelt conditions on the rock glacier. Extensive radar measurements on the rock glacier front over the whole year would be needed to confirm this assumption.

4.1.5 | Creep velocities: annual response

The creep rate of the Furggwanghorn rock glacier has increased substantially since observations began in the 1970s. Other authors have confirmed that relatively high creep rates were reached in comparison with other rock glaciers in the European Alps. Delaloye et al.[10,48] summarised annual creep rates of more than 30 rock glaciers from the European Alps, where displacements in the order of decimetres per year are reported. Bodin et al.[49] found a significant relationship between rock glacier deformation and ground temperature on the Laurichard rock glacier in the French Alps. Nevertheless, the acceleration of the creep rate of the Furggwanghorn rock glacier has slowed over the last 5 years, despite rising or almost constant ground temperatures.

It is apparent from the TLS-DEM comparisons that the average annual creep velocity has increased from the root of the rock glacier, with movements of less than 0.5 m y^{-1} (confirmed by GPS data at borehole F1 at 0.3 m y^{-1}) up to 6.5 m y^{-1} at the rock glacier front, where the advance is often combined with local failure. Displacements of up to 3 m y^{-1} were measured in the depression zone, with velocities between 2 and 3 m y^{-1} along the lateral edges. These findings are supported by point data from the GPS stations (although the inclinometer measurements were obtained before the GPS measurements commenced) and comparison of the photographs obtained from cameras K1 and K2. Regions exhibiting similar creep velocities are presented in Figure 12b with the corresponding creep directions. The results indicate that the movements of the rock glacier do not run parallel to the slope, with predefined paths, but are strongly affected by the local ground conditions and bedrock topography.

It is assumed that the measured creep velocities are composed of two parts: a relatively high annual base creep velocity and a small seasonal component, with a variable amplitude over the years. The increased base creep movements during the last decades are a consequence of the current climatic conditions in the higher altitudes of the Alps[50,51] and therefore the high temperatures within the rock glacier close to the thawing point.[21]

4.1.6 | Creep velocities: seasonal response

Seasonal creep dependency could be observed in a shear zone in the Muragl rock glacier (Grisons in Switzerland[17]) and is visible at the surface and in the shear zone for F5, F6 and F7 at Furggwanghorn (Figure 10). Although creep rates were sinusoidal in Muragl, the data are less consistent here. Rates tend to reduce after a specific cut-off point in winter, which ranges from December to February, probably linked to snow thickness (Figure 11), and increase during spring and summer. Data from the GPS stations for subsequent seasons (Figure 4) do not confirm this seasonality, although average creep rates agree well.

4.2 | Thermal-hydrological and mechanical interactions

The reasons for changes in the rate of seasonal creep are unclear despite extensive field investigations. Therefore, possible relationships between the current meteorology, the hydrological and thermal conditions in the ground and the creep at the surface may be examined (Figure 11). The creep velocities for the inclinometer (Figure 10) are given at the surface, because of the negligible changes between the shear zone and surface. Two main areas are differentiated: the surface and the shear zone.

Regarding the surface, Figure 11 shows that the TDR sensors at different depths reacted consistently to precipitation, as long as the surface was snow-free. Water contents rose abruptly during precipitation and then declined along a concave curve (point A). The water content correlated inversely with snow thickness. The decline of water content was caused by low air temperatures in winter, with snow thermally buffering the ground from the atmosphere. The start of the snow-melt period was marked by a rise in the water content (convex curve, point B).

For the shear zone, there were, unfortunately, no TDR sensors at that depth to establish a relationship between the water content and creep behaviour. Temperatures there remained almost constant while

the velocities changed. Temperature changes could only be detected at the beginning of the measuring interval of the inclinometers (September 2011) in boreholes F6 and F7, possibly due to drilling. Therefore, the temperature in the shear zone probably did not cause the velocity changes directly due to increasing susceptibility to creep at higher subzero temperatures, as predicted. Additionally, no direct correlation between the TDR sensors near the surface and the creep at the shear zone could be identified. These results are surprising, because an apparent seasonal effect can be seen for the creep velocities. However, how water influences the seasonal creep behaviour remains of debate.

Any correlation between precipitation and change in creep behaviour was examined in terms of a phase lag of up to several weeks. Although no direct correlation was found, it is assumed that the free pore water could have a major influence on the changes in creep velocity. First, warm permafrost close to the thawing point[21] together with the increased amount of water reduce the shear resistance of the soil-ice-water matrix.[13] Second, positive pore water pressure can occur, which will reduce the effective stresses locally and therefore the ground stability in general.

The depressions forming between boreholes F1 and F4 retained snow for much longer than elsewhere on the rock glacier. Therefore, infiltration of water occurred locally while the rock glacier was mainly snow-free and its hydrology was controlled by rainfall. Nevertheless, the influence of the water was probably partially delayed, due to heterogeneous ground and the various related flow paths within it.[22] However, this is difficult to prove. Stagnant water was observed in the depression south of borehole F3, while subsurface water was heard flowing multiple times in the root zone, although snowmelt had finished several weeks earlier and no recent precipitation had occurred.

The existence of positive pore water pressure of about 40 kPa at about 20 m depth was confirmed on September 7, 2010, while drilling borehole F3. It is assumed that liquid water can be stored temporarily within the rock glacier, perhaps for several weeks to months. Hence, water flow and storage within the rock glacier is not only a function of the permeability of the soil but also depends on the varying ice content[26] and the high ground temperature.

Despite such detailed investigations, some questions remain. The characterisation and monitoring of the rock glacier showed the complexity of the hydrological system on and within it. It is also hypothesised that the amount of water, due to either increasing ground temperature or precipitation, has a major influence on the deformation regime. Therefore, time-dependent measurements of the ice content and the pore water pressure at different depths and along the main flow directions would increase understanding of the internal processes.

5 | CONCLUSIONS

1. The Furggwanghorn rock glacier shows clear signs of advancing degradation, with continuing acceleration and deepening depressions in the root zone, supporting the findings of previous studies.
2. Complex, partially seasonal movements occurred on and within the rock glacier. Four shear zones were identified, one extending longitudinally over the entire rock glacier. The measurements confirmed that not all shear zones were active. The most visible changes occurred at the rock glacier root, where two parallel and transverse depressions deepened and surface instruments nearby rotated. Local rotation and deepening on the surface was explained by the geometry of the failure mechanisms, based on inclinometer and geophysical results. The creep behaviour in the acceleration zone below the depression zone was mostly translational, where creep velocity has increased substantially to up to 5 m y^{-1} in some locations, compared with displacements of about 1.5 m y^{-1} observed at the front in the 1970s.[25]
3. Two different failure regimes were identified at the front. First, base-level creep occurred year-round along the longest shear zones, as identified in three boreholes at depths between 15 and 20 m. This led to gradual steepening of most of the front slope and periodic failures of it, once the slope reached an inclination equal to a peak friction angle, whereupon the slope slumped back to an inclination represented by a critical state angle of friction of the debris. Second, seasonal failure was caused by water outflow on the front face due to snowmelt and heavy rainfall. This caused local failures by reducing effective stress, and possibly some undermining by erosion, as springs formed.
4. A 3-D conceptual model demonstrates the internal kinematic behaviour of a rock glacier, based on classical soil mechanics concepts.
5. The deformation of the rock glacier resulted from the complex internal structure and thermal-hydro-mechanical coupling between the atmosphere, snow, ice and soil matrix. Nevertheless, the inclinometer and thermistors within the same borehole did not show a direct link between changes in the displacement rate and ground temperature. Therefore, small temperature changes play a secondary role in influencing displacement rates directly for this rock glacier. It is hypothesized that the dominant gravitational forces in this fast-moving rock glacier mobilise shear forces in the shear zone that are not able to respond according to the expected relationship between ice temperature and shear resistance.[15,52]

ACKNOWLEDGEMENTS

Multidisciplinary field work was made possible through generous financial support from the ETH Research Commission (CHIRP project CHI-01 09-03). Canton Wallis (Charly Wuilloud and Pascal Stoebener) are also warmly thanked for their technical and financial contributions to the Furggwanghorn project. The local council in Gruben, Turtmanntal, is acknowledged for permitting the research team to carry out investigations. The authors gratefully acknowledge the many and varied contributions from their fellow researchers, who helped during this project, including Prof. Hansruedi Maurer, Prof. Wolfgang Kinzelbach, Prof. Fritz Stauffer, Dr Marian Hertrich, Dr Lasse Rabenstein and Dr Isabelle Gärtner-Roer, as well as the company Cheseaux SA that was responsible for drilling the boreholes in both campaigns. The contributions made by our highly skilled and committed technicians, especially Ernst Bleiker, Cornelius Senn, Marco Sperl, Thomy Keller, Heinz Buschor and Alfred Ehrbar were outstanding. Finally, we are most grateful to the associate editor, Dr Lukas Arenson,

the PPP editor, Professor Julian Murton, and the various expert reviewers, who made valuable suggestions regarding the manuscript.

ORCID

Thomas Buchli http://orcid.org/0000-0003-4216-1307
Kaspar Merz http://orcid.org/0000-0001-9215-6405

REFERENCES

1. Crosta GB, Chen H, Lee CF. Replay of the 1987 Val Pola landslide, Italian Alps. *Geomorphology*. 2004;60(1–2):127-146.
2. Krysiecki JM, Bodin X, Schoeneich P. Collapse of the Bérard Rock Glacier (Southern French Alps). In: Kane DL, Hinkel KM, eds. *Extended Abstracts of the Ninth International Conference on Permafrost*. University of Alaska Fairbanks; 2008:153-154.
3. Schoeneich P, Bodin X, Echelard T, et al. Velocity changes of rock glaciers and induced hazards. In: Dans Lollino G, Manconi A, Clague J, Shan W, Chiarle M, eds. *Engineering Geology for Society and Territory*. Climate Change and Engineering Geology (IAEG XII Congress, 15–19 Septembre 2014, Torino). berlin: Springer; 2014:223-227.
4. Bodin X, Krysiecki J-M, Schoeneich P, et al. The 2006 collapse of the Bérard Rock Glacier (Southern French Alps). *Permafrost Periglac Process*. 2017;28(1):209-223. https://doi.org/10.1002/ppp.1887
5. Arenson LU, Jakob M. Periglacial geo-hazard risks and ground temperature increases. In: Lollino G, Manconi A, Clague J, Shan W, Chiarle M, eds., *Engineering Geology for Society and Territory*. Vol 1. Cham: Springer International Publishing; 2015. doi: https://doi.org/10.1007/978-3-319-09300-0.
6. Kääb A, Frauenfelder R, Roer I. On the response of rockglacier creep to surface temperature increase. *Glo Planet Change*. 2007;56(1–2):172-187.
7. Kellerer-Pirklbauer A, Kaufmann V. About the relationship between rock glacier velocity and climate parameters in central Austria. *Austrian J Earth Sci*. 2012;105(2):94-112.
8. Zimmermann M, Haeberli W. Climatic change and debris flow activity in high-mountain areas—A case study in the Swiss Alps. Greenhouse-impact on cold-climate ecosystems and landscapes. *Catena* 1992;Suppl 22:59–72.
9. Haeberli W, Hallet B, Arenson LU, et al. Permafrost creep and rock glacier dynamics. *Permafrost Periglac Process*. 2006;17(3):189-214.
10. Delaloye R, Perruchoud E, Avian M, et al. Recent interannual variations of rock glacier creep in the European Alps. In: Kane DL, Hinkel KM, eds. *Proceedings of the Ninth International Conference on Permafrost*. University of Alaska Fairbanks; 2008:343-348.
11. Böckli L. *Characterizing Permafrost in the Entire European Alps: Spatial Distribution and Ice Content* [PhD thesis]. http://www.zora.uzh.ch/89504/. Accessed June 2016. Mathematisch-naturwissenschaftlichen Fakultät der Universität Zürich; 2013.
12. Davies MCR, Hamza O, Harris C. The effect of rise in mean annual temperature on the stability of rock slopes containing ice-filled discontinuities. *Permafrost Periglac Process*. 2001;12(1):137-144.
13. Arenson LU, Springman SM. Mathematical descriptions for the behaviour of ice-rich frozen soils at temperatures close to 0 °C. *Can Geotech J*. 2005;42(2):431-442.
14. Yamamoto Y, Springman SM. Three- and four-point bending tests on artificial frozen soil samples at temperatures close to 0°C. *Cold Reg Sci Technol*. 2017;134:20-32.
15. Arenson LU. Unstable Alpine Permafrost: a Potentially Important Natural Hazard [DSc thesis]. http://e-collection.library.ethz.ch/view/eth:25904. Accessed June 2016. *Institute for Geotechnical Engineering ETH Zurich*; 2002.
16. Wagner S. Creep of Alpine permafrost, investigated on the Murtèl rock glacier. *Permafrost Periglac Process*. 1992;3(2):157-162.
17. Arenson L, Hoelzle M, Springman S. Borehole deformation measurements and internal structure of some rock glaciers in Switzerland. *Permafrost Periglac Process*. 2002;13(2):117-135.
18. Krainer K, Bressan D, Dietre B, et al. A 10,300-year-old permafrost core from the active rock glacier Lazaun, southern Ötztal Alps (South Tyrol, northern Italy). *Quatern Res*. 2015;83(02):324-335.
19. Springman SM, Arenson LU, Yamamoto Y, et al. Multidisciplinary investigations on three rock glaciers in the Swiss Alps: legacies and future perspectives. *Geogr Ann A Phys Geogr*. 2012;94(2):215-243.
20. Springman SM, Yamamoto Y, Buchli T, et al. Rock glacier degradation and instabilities in the European Alps: a characterisation and monitoring experiment in the Turtmanntal, CH. In: Margottini C, Canuti P, Sassa K, eds. *Second World Landslide Forum*. Berlin: Springer; 2013:5-13.
21. Buchli T, Merz K, Zhou XH, Kinzelbach W, Springman SM. Characterization and monitoring of the Furggwanghorn Rock Glacier, Turtmann Valley, Switzerland: results from 2010 to 2012. *Vadose Zone J*. 2013;12(1). https://doi.org/10.2136/Vzj2012.0067
22. Zhou X, Buchli T, Kinzelbach W, Stauffer F, Springman SM. Analysis of thermal behaviour in the active layer of degrading mountain permafrost. *Permafrost Periglac Process*. 2015;26(1):39-56.
23. Escher A. Structure de la nappe du grand Saint-Bernhard entre Val de Bagnes et les Mischabels. *Rap Serv Hydr Géol Suisse*. 1988;7:
24. Merz K, Green AG, Buchli T, Springman SM, Maurer HR. A new 3-D thin-skinned rock glacier model based on helicopter GPR results from the Swiss Alps. *Geophys Res Lett*. 2015;42(11):4464-4472.
25. Roer I, Haeberli W, Avian M, et al. Observations and considerations on destabilizing active rock glaciers in the European Alps. In: Kane DL, Hinkel KM, eds. *Proceedings of the Ninth International Conference on Permafrost*. University of Alaska Fairbanks; 2008:1505-1510.
26. Merz K, Maurer HR, Buchli T, Horstmeyer H, Green AG, Springman SM. Evaluation of ground-based and helicopter ground-penetrating radar data acquired across an Alpine rock glacier. *Permafrost and Periglac Process*. 2015;26(1):13-27.
27. Merz K, Maurer HR, Rabenstein L, Buchli T, Springman SM, Zweifel M. Multidisciplinary geophysical investigations over an alpine rock glacier. *Geophysics*. 2016;81(1):WA147-WA157.
28. Optech ILRIS LR. Specification. http://www.optech.com/wp-content/uploads/ILRIS-LR-Spec-Sheet-140730-WEB.pdf. Accessed June 2016.
29. Rabatel A, Deline P, Jaillet S, Ravanel L. Rock falls in high-alpine rock walls quantified by terrestrial lidar measurements: a case study in the Mont Blanc area. *Geophys Res Lett*. 2008;35(10). https://doi.org/L10502
30. Jaboyedoff M, Oppikofer T, Abellán A, et al. Use of LIDAR in landslide investigations: a review. *Nat Haz*. 2012;61(1):5-28.
31. Swisstopo. Informationsbroschüre: Neue Koordinaten für die Schweiz, Der Bezugsrahmen LV95, Bundesamt für Landestopografie, Eidgenössische Vermessungsdirektion Geodäsie, Wabern. https://www.ag.ch/media/kanton_aargau/dvi/dokumente_5/arp_1/vermessungsamt_1/3__rechtliche_grundlagen_1/Der_Bezugsrahmen_LV95_Infobroschuere_der_swisstopo.pdf. *Accessed June 2016*. 2006;
32. Take WA. The Influence of Seasonal Moisture Cycles on Clay Slopes *[PhD dissertation]*. University of Cambridge; 2002.
33. White DJ, Take WA, Bolton MD. Soil deformation measurement using particle image velocimetry (PIV) and photogrammetry. *Géotechnique*. 2003;53(7):619-631.
34. Werner C, Wiesmann A, Strozzi T, Kos A, Caduff R, Wegmüller U. The GPRI multi-mode differential interferometric radar for ground-based observations. In: *Proceedings of the 9th European Conference on Synthetic Aperture Radar*; VDE Verlag; 2012:304-307.
35. Caduff R, Kos A, Schlunegger F, McArdell BW, Wiesmann A. Terrestrial radar interferometric measurement of hillslope deformation and atmospheric disturbances in the Illgraben Debris-flow catchment, Switzerland. *IEEE Geosci Remote Sensing Lett*. 11(2):434-438.
36. Caduff R, Schlunegger F, Kos A, Wiesmann A. A review of terrestrial radar interferometry for measuring surface change in the geosciences. *Earth Surf Process Landforms*. 2015;40(2):208-228.

37. Buchli T, Laue J, Springman SM. Amendments to interpretations of SAAF inclinometer data from the Furggwanghorn Rock Glacier, Turtmann Valley, Switzerland: results from 2010 to 2012. *Vadose Zone J*. 2016;15(4):15-14.
38. Leica Geosystems. CS10/CS15 and GS sensors, user manual, version 5. http://www.surveyequipment.com/PDFs/Leica_Viva_CS10_CS15_User_Manual.pdf. Accessed June 2016
39. Dach R, Hugentobler U, Fridez P, Meindl M. Bernese GPS Software Version 5.0. Astronomical Institute, University of Bern. http://www.bernese.unibe.ch/download50. *Accessed June 2016*; 2007.
40. Wirz V, Gruber S, Purves RS, et al. Short-term velocity variations at three rock glaciers and their relationship with meteorological conditions. *Earth Surf Dynamics*. 4:103-123.
41. Buchli T, Springman SM, Whittle R. Pressuremeter tests on a rock glacier in the Swiss Alps. In: *Proceedings of the 23rd European Young Geotechnical Engineering Conference in Barcelona (EYGEC)*; 2014:97-100 https://www.etcg.upc.edu/congressos/eygec-2014/docs/EYGEC2014.pdf. Accessed June 2016.
42. Cook FA, Albaugh DS, Brown LD, Kaufman S, Oliver JE, Hatcher RD. Thin-skinned tectonics in the crystalline southern Appalachians; COCORP seismic-reflection profiling of the Blue Ridge and Piedmont. *Geology*. 1979;7(12):563-567.
43. Boyer SE, Elliott D. Thrust systems. *American Association of Petroleum Geologists*. 1982;66:196-1230.
44. Terzaghi K. *Theoretical Soil Mechanics*. 510 Chichester: John Wiley & Sons; 1948.
45. Yamamoto Y, Springman SM. Axial compression stress path tests on artificial frozen soil samples in a triaxial device at temperatures just below 0 °C. *Can Geotech J*. 2014;51(10):1178-1195.
46. Terzaghi K. *Erdbaumechanik auf bodenphysikalischer Grundlage*. Leipzig: Franz Deuticke, Leibzig und Wien; 1925.
47. Andersland OB, Ladanyi B. *An Introduction to Frozen Ground Engineering*. 1st ed. Dordrecht, The Netherlands: Springer Science and Business Media; 1994.
48. Delaloye R, Lambiel C, Gärtner-Roer I. Overview of rock glacier kinematics research in the Swiss Alps. *Geogr Helv*. 2010;65(2):135-145.
49. Bodin X, Thibert E, Fabre D, et al. Two decades of responses (1986-2006) to climate by the Laurichard rock glacier, French Alps. *Permafrost Periglac Process*. 2009;20(4):331-344.
50. Vaughan DG, Comiso JC, Allison I, et al. Observations: cryosphere. In: Stocker TF, Qin D, Plattner GK, et al., eds. Climate Change 2013: The Physical Science Basis. Contribution of Working Group I to the Fifth Assessment Report of the Intergovernmental Panel on Climate Change. Cambridge, UK: Cambridge University Press; 2013.
51. Roer I, Kääb A, Dikau R. Rockglacier kinematics derived from small-scale aerial photography and digital airborne pushbroom imagery. *Z Geomorphol*. 2005;49(1):73-87.
52. Yamamoto Y. *Instabilities in Alpine Permafrost. Strength and Stiffness in a Warming Regime* [DSc thesis]. http://e-collection.library.ethz.ch/view/eth:25904. Accessed June 2016. Institute for Geotechnical Engineering ETH Zurich; 2013.

SUPPORTING INFORMATION

Additional Supporting Information may be found online in the supporting information tab for this article.

How to cite this article: Buchli T, Kos A, Limpach P, Merz K, Zhou X, Springman SM. Kinematic investigations on the Furggwanghorn Rock Glacier, Switzerland. *Permafrost and Periglac Process*. 2018;29:3–20. https://doi.org/10.1002/ppp.1968